ACS APPLIED MATERIALS & INTERFACES

Research Article

www.acsami.org

In Situ Wetting State Transition on Micro- and Nanostructured Surfaces at High Temperature

Jingming Wang,*[,†] Meng Liu,[†] Rui Ma,[†] Qianbin Wang,[†] and Lei Jiang[†,†]

[†]Key Laboratory of Bio-Inspired Smart Interfacial Science and Technology of Ministry of Education School of Chemistry and Environment, Beihang University Beijing 100191, P.R. China

[†]Beijing National Laboratory for Molecular Sciences Key Laboratory of Organic Solids, Institute of Chemistry Chinese Academy of Science, Beijing 100190, P.R. China

Supporting Information

ABSTRACT: We studied the in situ transition of the droplets' wetting state on the heated solid surfaces. The wetting behaviors of four micro- and nanostructured surfaces with different chemical components were studied. These parameters included the maximum contact areas (MCA), the maximum evaporation areas (MEA) and the wetting transition temperature (T_{trans}). The reduction in MEAs has a specific transition process from wetting (Wenzel state) or partial wetting (Wenzel-Cassie intermediate state) to nonwetting (Cassie State) as the surface temperature rises. When the MEAs drop to zero at a critical temperature (T_{trans}), the droplets rebound from the heated surfaces to complete the wetting transition process. The chemical compounds and the surfaces' rough structure play an important role in the droplets' wetting transition behavior. Before FAS-modification, microstructures can increase the MCAs, MEAs, and T_{trans}. However, the microstructures are less effective at increasing the MEAs and T_{trans} than changes to nanostructures. After FAS-modification, both the nano- and microstructures reduce the T_{trans}. On the FAS-MNSi surfaces, the MEAs are always zero—the droplets rebounded at room temperature, and the wetting transition did occur. We propose two high-temperature mechanisms to explain these transition phenomena.

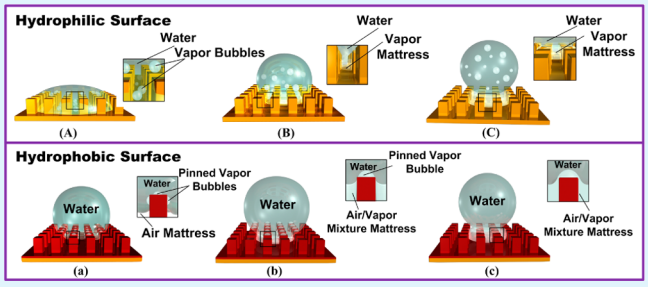

KEYWORDS: *wetting state transition, nanostructure, microstructure, rebound, vapor bubble*

1. INTRODUCTION

Heat transfer is of great importance in many industrial processes such as chemical processing, electronic devices, and nuclear power plants.[1,2] Boiling heat transfer is particularly important and has been widely applied to industry cooling systems.[3−5] Spray cooling is an emerging and effective cooling technique that transfers the substantial heat of evaporation by absorbing large amounts of thermal energy from a hot surface.[6,7] During spray cooling, most heat removal is done through nucleate boiling, which starts in micro- and nanocavities as nucleation sites. From these sites, the liquid reaches temperatures above their saturation value and forms steam bubbles to carry the thermal energy from the heated surface to the surrounding space.[8]

Recent studies show that the heat transfer efficiency of the spray cooling process depends largely on the surface roughness including micropores,[9] microchannels,[10,11] nanowires,[12] and nanorods.[13] Rough structures may accelerate the nucleation rate and increase the number of nucleation sites. Rough structures also markedly change the wettability of hot surfaces.[14−17] If the surface wettability changed, the wetting state between the liquid and heated solid surface would be changed dramatically.[18−20] This would alter the activation of nucleation sites. However, the explanation above is not adequate to explain the extremely high heat transfer efficiencies observed for heated solid surfaces with rough structures. It needs more in depth study.[21]

To do this, researchers have studied single droplets impinging on a hot surface as a model of the cooling behavior of sprays.[22] As the droplet impacts the heated solid surface, heat is transferred from the solid to the liquid phase. This energy transfer to the droplet increases its mean temperature, and liquid vaporizes from the bottom of the droplet. If the heat transfer rate is large enough during impact, the liquid is vaporized. The droplet forms a vapor layer between the solid and the liquid phase, which repels the droplet from the solid surface. This is the wetting state transition.

Heat transfer is minimized minimum and the evaporation lifetime of the droplet is maximized in the wetting transition. This phenomenon is known as the Leidenfrost effect.[23−25] Therefore, there is much work focusing on the wetting transition behavior of the droplets on heated solid surfaces.[26,27] The experimental results demonstrate that rough structures and

Received: June 3, 2014
Accepted: August 20, 2014
Published: August 20, 2014

chemical components on the heated solid surfaces have a great influence on the wetting transition temperature.[28−31]

The wetting transition temperature can be improved by increasing the surface roughness and decreasing the surface energy. However, studying the wetting transition temperature on heated solid surfaces is inadequate to understand the cooling behavior of sprays. The wetting transition process on the heated solid surface, especially the effect of chemical components and different scaled structures on the wetting transition processes, is much more important for the heat transfer process of sprays.

Herein, we report a study of the in situ transition processes of droplets wetting state on four kinds of micro- and nanostructured surfaces with different chemical components from 23 to 300 °C. The wetting behaviors of liquid droplets on the heated solid surfaces were observed including the maximum contact areas (MCA), the maximum evaporation areas (MEA) and the wetting transition temperature (T_{trans}). The reduction in the MEAs is a specific transition process from wetting (Wenzel state) or partial wetting (Wenzel−Cassie intermediate state) to nonwetting (Cassie State) when the surface temperature rises. When the MEAs drop to zero at a critical temperature (T_{trans}), the droplets rebound from the heated surfaces to complete the wetting transition. Chemical compounds and roughness of the surface play important roles in the droplets' wetting transition. Before FAS-modification, microstructures can increase the MCAs the MEAs and T_{trans}, which are more useful to promote the MCAs especially on the relative high temperatures that are close to T_{trans}. However, the microstructures are less effective at increasing the MEAs and T_{trans} than the nanostructures. After FAS-modification, both nano- and microstructures will reduce the T_{trans}. On the FAS-MNSi surfaces, the MEAs were always zero. That is, the droplets rebounded at room temperature, and the wetting transition did not take place.

2. EXPERIMENTAL SECTION

Instruments and Characterization. A Quanta 250 environmental SEM (FEG, USA) obtained the top view images. Equilibrium CA measurements were made using an OCA 20 instrument (DataPhysics, Germany) at 25 °C. Side-view images of the droplets contacting with the heat surfaces were captured through high-speed camera (HSCCD, V9.1, PHANTDM, USA).

Fabrication of Silicon Micropillar Arrays. An ordered array of micropillar structures was fabricated using photolithography. A contact lithographic mask was obtained from the Institute of Microelectronics of the Chinese Academy of Sciences (Beijing, China). The mask aligner/exposure system (Karl Suss MA6, Germany) transferred mask micropatterns onto silicon wafers. The deep etching process was completed using an etch system (STS ICP ASE, U.K.).

Fabrication of Silicon Nanowire Arrays. Smooth silicon strips were soaked in the mixed solution of H_2SO_4/H_2O_2 ($V[H_2SO_4(97\%)]/V[H_2O_2(30\%)] = 3:1$) for 1 h at 80 °C. They were then rinsed with deionized water four or five times. The clean silicon strips had been immersed in a Teflon-lined stainless steel autoclave with etching solution containing 15 mL of HF, 35 mL of deionized water, and 0.1699 g of $AgNO_3$ for 10 min at 50 °C. After etching, the strips were dipped into 20% nitric acid for 30 s until the upper white film disappeared. They were finally rinsed with deionized water four or five times.

Modification with FAS. Silicon strips with various structures were put into a sealed container together with a piece of glass covered with 20 μL FAS. The air in the container was then evacuated with a vacuum pump, and the vacuum was maintained for 12 h.

Wetting Transition Process. A schematic diagram of the experimental device is shown in the Supporting Information, Figure S1. A heating stage with controllable temperature was used; the surface temperature was monitored with a precise thermocouple. The pinhead of the injector needle was kept 200 mm higher than the heating stage to protect the drop from heat. Only when the stage temperature reaches the test temperature was the surface moved down. Then, a water droplet with 2 mm diameter was generated on a hydrophobic needle with a syringe driven by a PHD 2000 infusion and withdrawal pump (Harvard, USA) at 0.05 mL/min. Then water droplets were released at a height of 3.5 mm to impact the heated surface. After the water droplet left the injector needle, the heated surfaces were moved up to the new high position. The temperature of water drops could be kept at 29 °C before coming into contact with the high-temperature surfaces (see the Supporting Information, S2) Simultaneously, the side-view images of the droplet were captured.

3. RESULTS AND DISCUSSION

Silicon substrates with various structures and chemical compounds were selected to investigate the in situ wetting transition behavior of a water droplet at different temperatures. Figure 1 shows the top-view scanning electron microscope (SEM) images and the static contact angle (CA) images of a water droplet before and after chemical modification with FAS at 25 °C. As shown in Figure 1a, the unmodified smooth silicon substrate (SSis) exhibited hydrophilic characteristics with a CA of 19.8 ± 1.6°, The FAS-modified SSis (FAS-SSis) was hydrophobic (CA 110.0 ± 0.5°). After 150−200 nm and 4.82 μm nanowire arrays (see the Supporting Information, Figure S4a) were fabricated on the SSis, the unmodified nanostructured silicon surface (NSis) achieved superhydrophilicity with a CA near 0°.The corresponding FAS-modified NSis

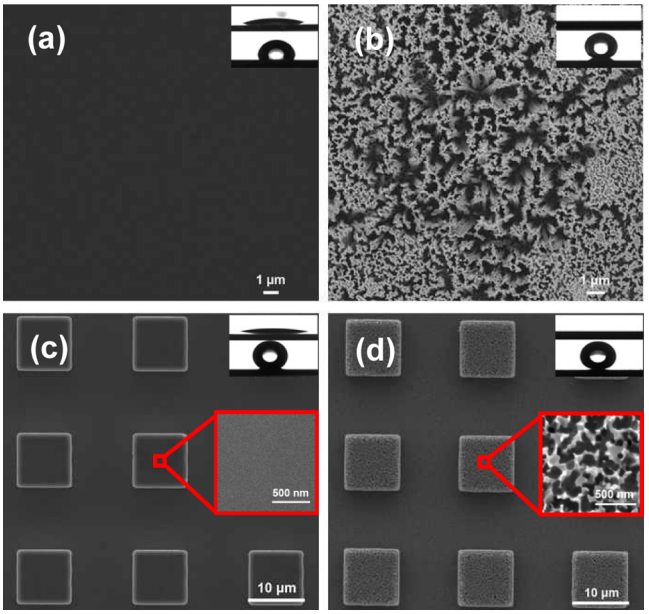

Figure 1. SEM images of silicon surfaces with different scaled structures as well as contact angle illustrations of water droplets on these surfaces before (top) and after (bottom) FAS modification. (a) SSis, CA (19.8 ± 1.6)°/(110.0 ± 0.5)° (before/after modification). (b) Silicon substrate with nanowire arrays, CA 0°/(151.2 ± 0.4)°. (c) Silicon substrate with micropillars at W/H/D (width/height/spacing of the micropillars) 10/5/10 μm and CA (13.8 ± 3.1)°/(145.7 ± 0.6)°. The inset shows the smooth surface on the top view of a micropillar at higher magnification. (d) Silicon substrates with the composition of nanowire arrays and micropillars. The W/H/D is 10/5/10 μm and CA 0°/(155.4 ± 0.7)°. The inset shows the nanowire arrays on the top view of a micropillar at higher magnification.

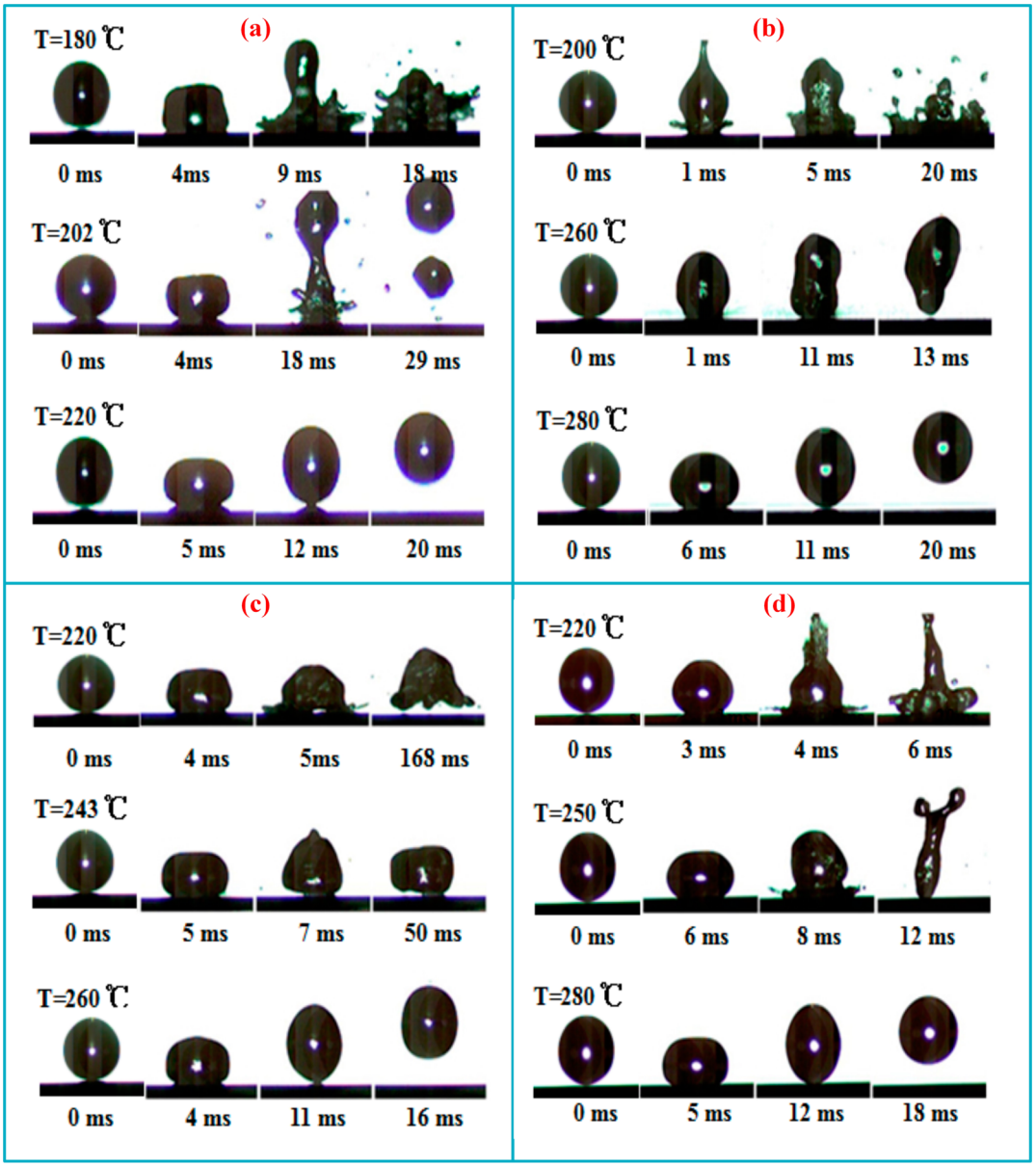

Figure 2. Series of video snapshots of representative water droplet impacts on the four kinds of unmodified surfaces at various surface temperatures. (a) SSis, (b) silicon substrate with nanowire arrays, (c) silicon substrate with micropillars (W/H/D 10/5/10 μm), and (d) silicon substrate with a composition of nanowire arrays and micropillars (W/H/D 10/5/10 μm).

(FAS-NSis) showed superhydrophobicity (CA > 150°) (Figure 1b).

When using micropillar arrays with smooth surfaces, the microstructured silicon surfaces (MSis) were hydrophilic (CA ≈ 13.8°) and superhydrophobic before and after FAS modification, respectively (Figure 1c). Correspondingly, the nanostructured MSis (MNSis) could be superhydrophilic before modification (Figure 1d), whereas the FAS-modified MNSis (FAS-MNSis) were superhydrophobic (CA >150°; slide angle <5°) such that the 3 μL water droplet could easily escape. The width/height of the micropillars selected in Figure 1c, d was about 10/5 μm. The spacing between the micropillars was 10 μm (more details, see the Supporting Information, Figures S3−S6).

Subsequently, the in situ wetting transition processes of water droplets on the surfaces including SSis, NSis, MSis, MNSis, FAS-SSis, FAS-NSis, FAS-MSis, and FAS-MNSis at various surface temperatures were investigated. For all runs, the properties of the droplets before surface impact held constant as were the droplet diameter and impact velocity.[32] By neglecting the deviation of drop shape from sphere due to oscillations and the force acting on the drop, the variation of the droplet impact velocity u_0 with the droplet height H can be calculated using eq 1 as follows[33]

$$u_0 = \sqrt{2g(H - D_0)} \tag{1}$$

After the water droplets delivered from the needle tip were made to impact on the heated surfaces, the droplet impact condition can be represented using W_e and R_e in eq 2.

$$W_e = \frac{\rho {u_0}^2 D_0}{\sigma} \text{ or } R_e = \frac{\rho u_0 D_0}{u} \tag{2}$$

dx.doi.org/10.1021/am5034457 | ACS Appl. Mater. Interfaces 2014, 6, 15198−15208

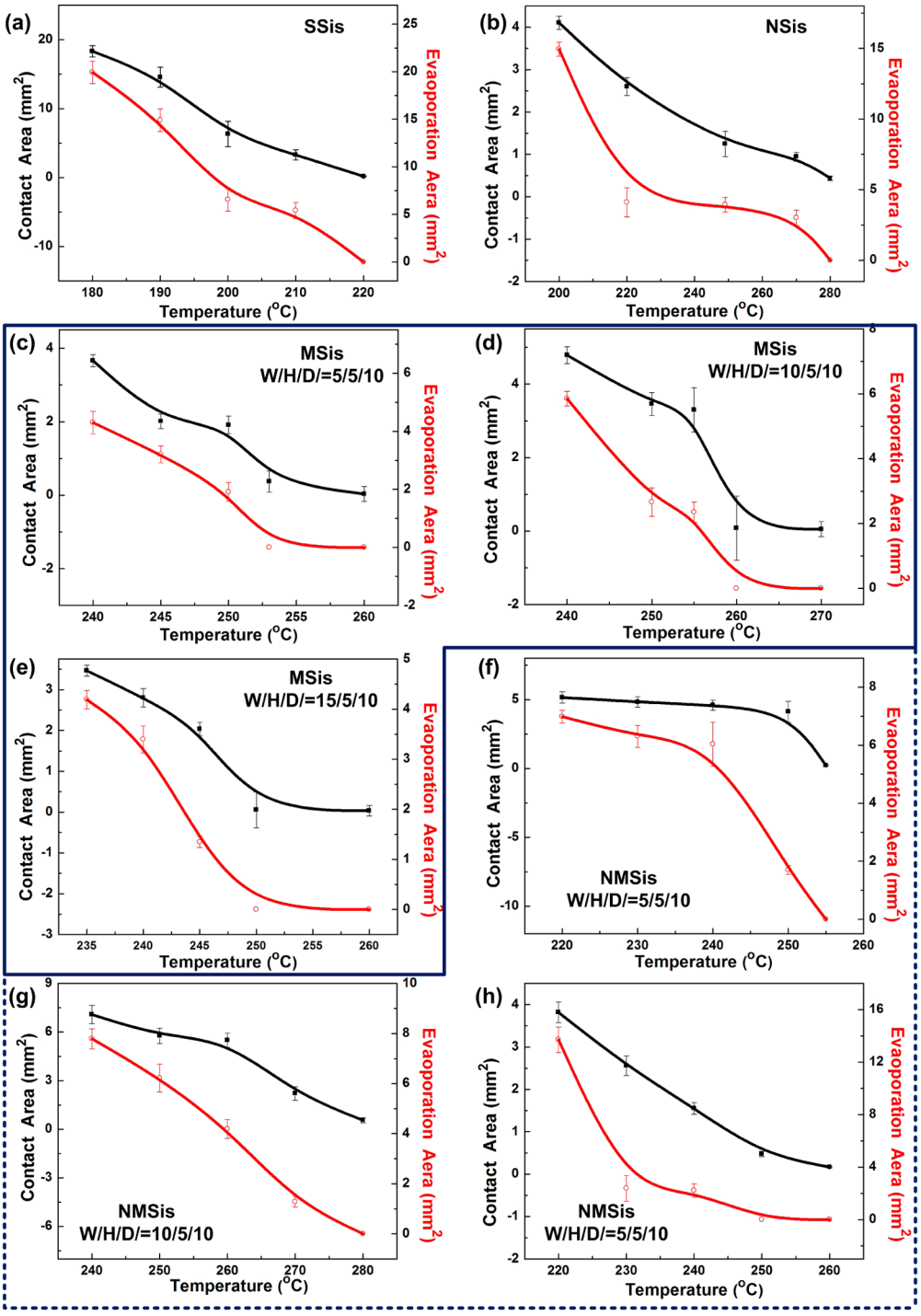

Figure 3. Variation in the maximum contact (■) and evaporation (□) area of the droplets of unmodified (a) SSis, (b) NSis, (c–e) MSis, and (f–h) MNSis.

Where u_0 and D_0 are the droplet impinging velocity and the droplet diameter before impingement. ρ, σ and μ are droplet density, droplet surface tension and droplet viscosity in the room temperature, respectively. That is to say, ρ = 998 kg/m^3, $\sigma = 72 \times 10^{-3}$ N/m, and $\mu = 1.0050 \times 10^{-3}$ Pa s. Thus, W_e and R_e are 0.815 and 522.8, respectively.

Figure 2 illustrates a series of video snapshots of representative water droplet impacts on the four unmodified surfaces with various microstructures at increasing surface temperatures (SSis, NSis, MSis, MNSis).

We first studied unmodified hydrophilic SSis surface (Figure 2a) with the surface heated to 180 °C or above. Here, shortly after the droplet impacted the surface, the upper part of the droplets ejected upward while the bottom made contact with the surface and formed lamella. After the lamella expanded, the upper part of the droplets fell down on the liquid and tiny droplets were ejected from its periphery. By increasing the surface temperature to 200 °C, these ejections were much higher and achieved a narrow neck on the central droplet. This decreased the contact area between the bottom of the droplet

dx.doi.org/10.1021/am5034457 | ACS Appl. Mater. Interfaces 2014, 6, 15198–15208

and the heated surface. Later, the upper half of the droplet finally detached from the lower half and both halves bounced.

When the surface temperature was 220 °C, the droplet bounced up directly after it made contact with the surface. Similarly, if the droplet impacted the superhydrohilic NSis surface (Figure 2b) at a lower temperature (200 °C), the upper part of the droplets would eject upward leaving the bottom to splash on the heated surface. A collapse occurred after the ejected part of the droplet fell down. When the surface temperature rose to 260 °C, the upper half of the droplet jetted to make a wide neck on the central section. It then left the heated surface upward with a large head and a thick tail. If the surface temperature increased much higher (280 °C), the process would rebound. In comparison, the droplet ejection was not distinct on the heated hydrophilic MSis surface (Figure 2c). When the surface temperature was 260 °C, the droplet rebounded. The intense jets of the droplets achieved on the MNSis surfaces.

Shortly after impacting the surface at 220 °C, a fountain came to the top of the droplet and its bottom splashed on the heated surface. A few milliseconds later, we noted subsidence on the lower part of the droplet and an ejection came through the liquid layer. As the surface temperature increased, the fountain disappeared from the droplet leaving only the splash underneath it. Subsequently, a central jet formed (Figure 2d). According to the results above, this ejection will form much more easily on the SSis, NSis surfaces than on MSis.

The vapor pressure generally increases abruptly and disrupts the liquid's bottom surface. Violent, sometimes explosive, ejection of droplets (large or tiny) due to the venting of the vapor bubbles can also occur.[23] Therefore, vapor bubble parameters (number, size and shape) are crucial to understanding the wetting transition behaviors of water droplets that are in turn influenced greatly by rough structures and wettability.[34] The vapor bubbles form much more easily on rough surfaces with nanowire arrays (NSis and MNSis surface) than on smooth one because the nanostructures provide more cavities for bubble nucleation.[35] Thus, ejection is seen on the NSis and MNSis surfaces rather than the MSis surface. Indeed, the more hydrophilic the surfaces are, the fewer bubble adhesion forces they exhibit. Thus, many vapor bubbles do not grow to larger ones before leaving the superhydrophilic surfaces. This leads to splashing on the NSis and MNSis surfaces.[36,37]

Contact between a droplet and the heated surfaces leads to the formation and growth of many vapor bubbles and consequently a high rate of heat transfer from the heated surface. Because of the polydispersity of the venting vapor bubbles, the evaporation processes changes when performed on different surfaces. This generally determines the heat-transfer ability of the heated surface.[38] Therefore, the maximum contact and evaporation area of the droplets were both investigated (Figure 3). Here the maximum contact area (MCA) is the maximum area where the droplet liquid spreads out radially from the impact point until the droplet velocity at vertical direction reach zero, whereas the maximum evaporation area (MEA) is the maximum area where the drop liquid is at a maximum drop spread and the spread velocity at horizontal direction reach zero.

On the SSis surface, the maximum contact area (MCA) is ~20 mm^2 at relatively low surface temperature (180 °C). This decreased with rising surface temperature until it was nearly zero at 220 °C (Figure 3a). The MEA on the SSis surfaces were always similar to the MCAs before the droplets rebounded from the heated SSis surfaces. MEA also decreased with surface temperature increase. This demonstrates that the vented vapor bubbles could not change the MEAs after the water droplets contacted the heated SSis surface.

The MEA reduction illustrates a specific transition process that starts from the wetting (Wenzel state) to nonwetting (Cassie state). When the MEAs dropped to zero, the surfaces were nonwetting and the wetting transition process quickly finished. Comparing to the SSis surfaces, the NSis surfaces had special wetting phenomena. First, both the MCAs and MEAs on the NSis surfaces decreased with rising surface temperature. In contrast, the MEAs were much larger than the MCAs before the droplets rebounding from the heated surfaces. Second, the T_{trans}, (the temperature at which the MEAs reach zero) is higher than that on SSis surface. This may be caused by the nanostructures, which provide more cavities for bubble nucleation and thus form more vapor bubbles on the NSis surface. Although the large amount of vented tiny vapor bubbles would enhance the disturbance of the droplets and increase the MEAs (versus the SSis surface), it is quite difficult for the vapor bubbles to coalescence with each other since they could not stay on the hydrophilic surfaces. Thus, the T_{trans} rose significantly. In fact, the nanostructure, including nanofiber,[39] nanoporosity,[28] and nanotube[40] is the crucial feature in efficiently increasing the T_{trans} by initiating heterogeneous nucleation of bubbles during short-lived solid−liquid contacts, which results in disruption of vapor film.

When the SSis surface used microstructures, the behavior of the droplets at different surface temperatures was more complicated (Figure 3c, d). The MCAs and MEAs decreased with the rising surface temperature, and the MEAs dropped faster than the MCAs did. That is, on the MSis surfaces, the MEAs were larger than the MCAs at a relatively low surface temperature (<240 °C). The MEAs were smaller than the MCAs at a relatively high surface temperature until the droplets rebounded from the surface. The results showed that the microstructures increase the MCAs and the MEAs, and they increase the MCAs especially at relatively high temperatures close to T_{trans}.

However, the microstructures were less effective on increasing MEAs than the nanostructures. This may be because there were fewer vented vapor bubbles on the MSis surfaces than on NSis surfaces. Furthermore, the size of the microstructures played an important role on the droplet transition. The MCAs, MEAs and T_{trans} on the ~10 μm wide micropillars were the highest (Figure 3d), whereas those 15 μm wide were the lowest (Figure 3c).

If the nanowire arrays were constructed on the MSis surface (i.e., MNSis surface), the MCAs, MEAs and T_{trans} trends were similar to those seen on the MSis surface (Figure 3e-g). The larger the nanowire array areas, the more the MCAs and MEAs were improved. However, T_{trans} did not increase markedly except for the T_{trans} on the MNSis surface with micropillar widths of ~10 μm. Furthermore, the MCAs, MEAs and T_{trans} on the MNSis surface with ~10 μm micropillars were the highest (Figure 3f), and the ~15 μm sample was the lowest (Figure 3g). Therefore, when the micro/nano-hierarchical rough structures were induced, the MCAs and MEAs could be increased even if the surfaces were hot.

The droplet behaviors on the FAS-modified surfaces were investigated because the surface chemical compound would markedly influence surface wettability.[41] A series of video

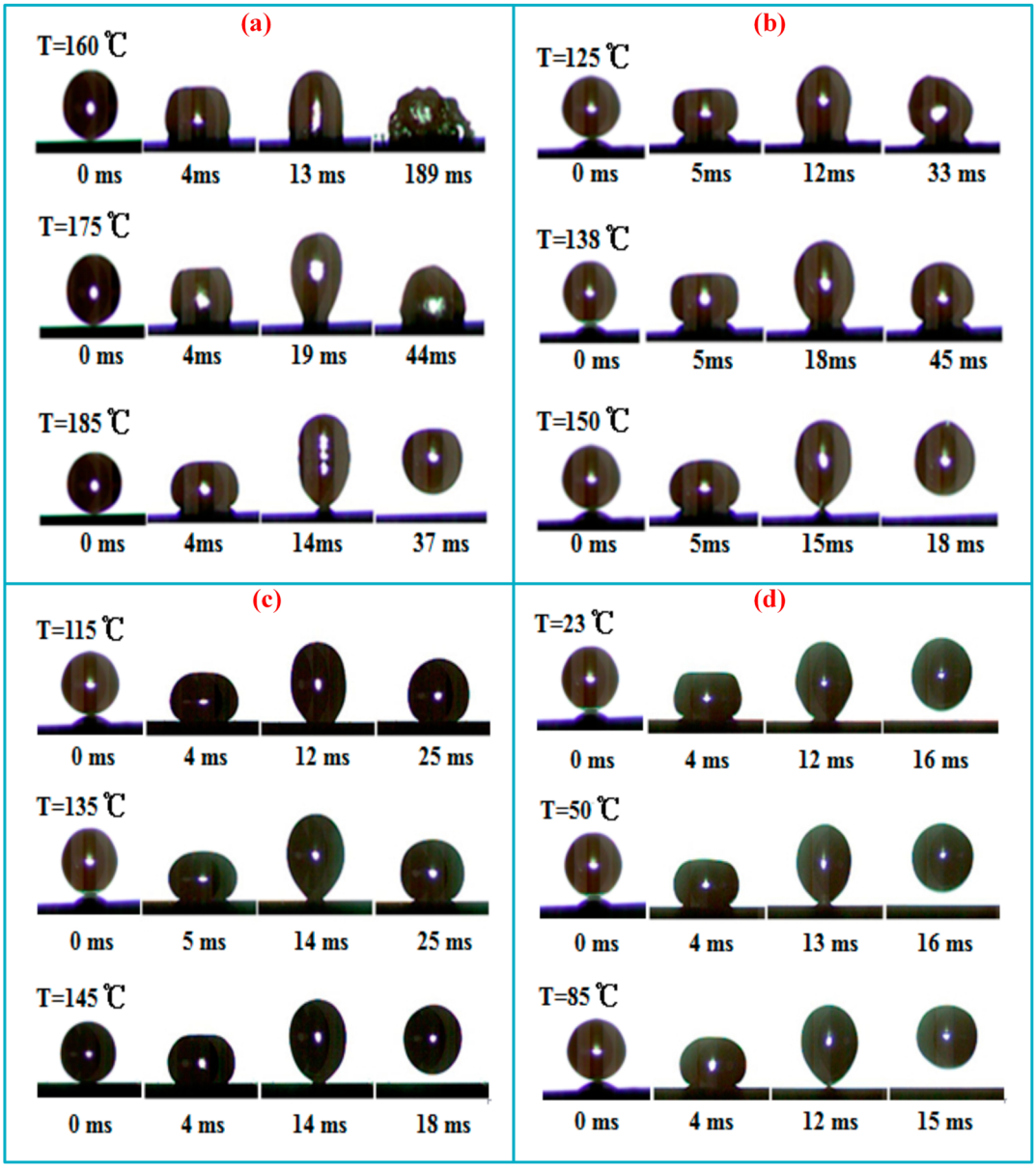

Figure 4. Series of video snapshots of representative water droplet impacts on the four FAS-modified surfaces at various surface temperatures. (a) SSis, (b) silicon substrate with nanowire arrays, (c) silicon substrate with micropillars (W/H/D 10/5/10 μm), (d) silicon substrate with composition of nanowire arrays and micropillars (W/H/D 10/5/10 μm).

snapshots of representative water droplet impacts on the FAS-SSis, FAS-NSis, FAS-MSis, and FAS-MNSis at increasing surface temperatures are shown in Figure 4. Figure 4a shows images for an experiment using FAS-SSis. The side views in these images clearly show that shortly after impact, the droplets tried to move upward, whereas the bottom stuck to the surface at a relative low temperature. Then the contact area expanded. This leads to a high rate of heat transfer from the heated surface and consequently forms vapor bubbles. The vapor pressure increased abruptly causing venting of the vapor bubbles and subsequent disruption of the liquid's bottom surface. If the surface was heated to 175 °C, the initial pinning area of the droplet decreased and the droplet height increased. The evaporation area dropped and there was no obvious disruption of the liquid's bottom surface because of the thicker vapor layer. When the surface temperature was high enough (>185 °C), the vapor layer is sufficiently thick to prevent the liquid from touching the surface. The initial pinning area was minimal (nearly zero), and the droplet rebound from the heated surfaces was due to expansion of vapor bubbles.

If the droplet impacted the superhydrophobic FAS-NSis surface (Figure 4b) at a lower temperature (125 °C), the droplet would move upward a bit, leaving the bottom pinning with a wide neck on the heated surface. The nanostructures provided more nucleation sites for vapor bubbles. Thus, the vapor layer would be thickened, which prevented the droplet from spreading on the heated surface at low temperatures. More vapor bubbles were generated on the heated FAS-NSis surfaces as the surface temperature increased. Thus, the neck on the bottom of the droplet shrunk, and the droplets did not spread out at all.

The droplet neck disappeared and the rebounding process occurred if the surface temperature increased to 150 °C or more. The droplet behavior was similar to that on the FAS-

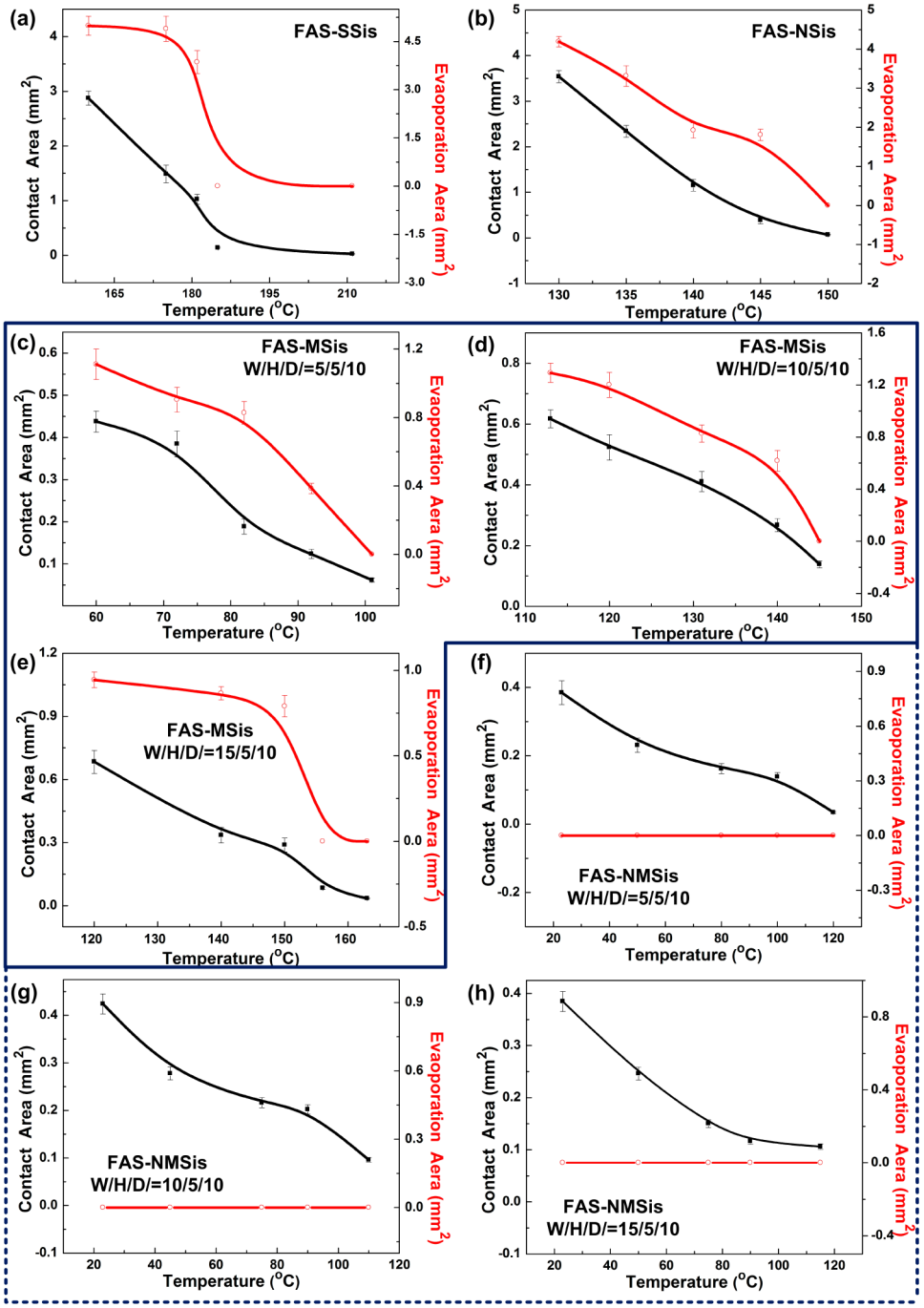

Figure 5. Variation in the maximum contact (■) and evaporation (□) area of the droplets of FAS-modified (a) SSis, (b) NSis, (c–e) MSis, and (f–h) MNSis.

NSis surface when the microstructures were constructed on silicon surfaces (Figure 4c). However, during droplet contact and evaporation, the neck on the bottom of the droplets could not be seen on the FAS-MSis surfaces. The spaces in the microstructures could not only trap air, but could also provide enough room for the growth or coalescence of the vapor bubbles. This continuous and thin gas layer created the droplet pinning effect. If the surface temperature was high enough, the pinning area shrunk to zero, and the droplets rebounded from the heated surface. If the micro/nano-hierarchical structures were introduced to the FAS-modified silicon surface, enough vapor bubbles nucleation sites could be provided by the nanostructures. Moreover, the air layer trapped in the micro/nano-hierarchical structures was thick enough to prevent droplet pinning. Therefore, the pinning area of the FAS-MNSis surface dropped markedly, and the droplets bounced even at room temperature.

We also studied the droplets' MCAs and MEAs because they are two critical parameters of heat transfer (Figure 5). On the FAS-Sis (Figure 5a), FAS-NSis (Figure 5b) and FAS-MSis (Figure 5c–e) surfaces, the variation of the MCAs and MEAs were similar. The MCAs and MEAs decreased with rising surface temperatures. The MEAs were far larger than the MCAs until the droplet rebounded from the surfaces and the MEAs dropped to zero. Before rebounding, the droplets partially wetted the surface (i.e., Wenzel–Cassie intermediate state). At

dx.doi.org/10.1021/am5034457 | ACS Appl. Mater. Interfaces 2014, 6, 15198–15208

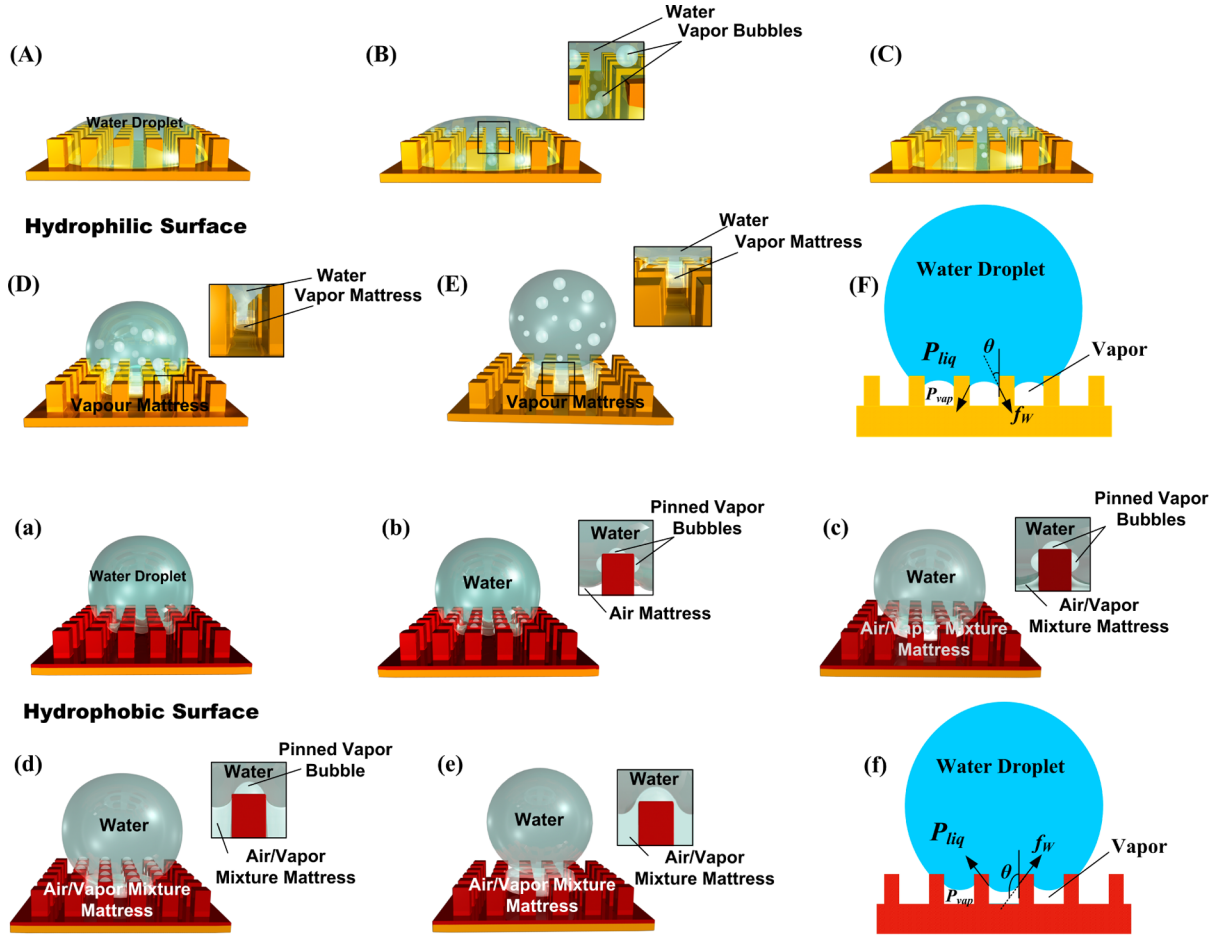

Figure 6. Schematic model of the wetting transition behavior of liquid droplets on the rough surfaces (A–F) without and (a–f) with FAS modification. (A) Hydrophilic surface at room temperature (Wenzel state). (B, C) Turbulent liquid droplets generated by venting of the vapor bubbles that are generated at the contact areas between the liquid and surface. (D) Vapor bubbles coalesce to form a vapor mattress that prevents the droplet and the surface from contacting, and the droplet moves up. (E) Droplet is blocked by the vapor mattress and bounces from the surface. (F) The scheme of the possible contact state of Wenzel droplet. (a) Hydrophobic surface at room temperature (Cassie state). (b) Vapor bubbles generate a limit contact area and then pin the contact area. The tiny vapor bubbles cannot coalesce with the air mattress, and the liquid droplets stand at the rough surface. (c, d) Pinned vapor bubbles grow in site and coalesce with the trapped air layer to form a mixture mattress when the three contact phase lines moves up. (e) When TPCL move to the top of the rough structures, the pinned vapor bubbles on the top coalesce with the gas mixture mattress to form a continuous gas layer that prevents contact between the liquid and the surface. The droplet then rebounds from the surface. (f) Scheme of the possible contact state of Cassie droplet.

relatively higher temperatures, the disruption of the liquid's bottom surface expanded the MEAs because of vapor bubble venting.

When the gas layer was continuous and thick the MEAs would drop to zero and the droplets became bound. The droplets changed to nonwetting (Cassie state). We also found that rough structures can greatly influence the in site changing of the droplets. The nano- and microstructures best reduced the T_{trans} when the micropillars are ~5 μm wide. Although nanowires could provide more nucleation cites for vapor bubbles, the vapor bubbles adhered on the tips of the nanowires, and could not form continuous vapor layers if the surface temperature was not high enough. The spaces between the microstructures were more useful at entrapping air to form a thick air layer. The smaller the micropillars, the easier it was to form a continuous gas layer. If the micro/nano hierarchical structures were constructed, the gas layer could be form at very low temperatures. Thus, on the FAS-MNSis surfaces, we found that the MCAs are reduced with increasing surface temperature. The MEAs were always zero. The droplets rebounded at room temperature and the wetting transition process could not be investigated (Figure 5g, h).

As known, the impact velocity, i.e., the impact Reynolds and Weber numbers, has a remarkable influence on the dynamic behavior of droplet impacting onto heated surfaces. And there are a number of works focusing on the effect of impact velocity on the dynamic behavior of droplet impacting (i.e., the dependence of β_{max} on W_e and R_e), which are illustrated in the Supporting Information, S7. However, the dynamic behavior of droplet impacting onto heated surface may be affected by surfaces components[42] and surface roughness.[39,28,40,43,44] However, there are few works that have systematically considered the inflences of chemical components and different scaled structures, including microscaled, nanoscaled, and micronanocomposited structures, on the droplet behaviors on heated surfaces at the same time.

Therefore, the droplet impact conditions are kept constant, and the surface character including the surfaces temperature, chemical compounds, and micro/nano rough structures, which result in the wetting in site transition process, were investigated

here. We propose a model to focus on understanding the influence of chemical compounds and micro/nano rough structures on the wetting transition process (Figure 6).

On the unmodified rough structures, the structures can be wetted at room temperature, and the surface is hydrophilic, i.e., the droplet is at a Wenzel state (Figure 6A). When the surfaces temperature rises, vapor bubbles are generated at the contact rough area between the liquid and surface. The droplet may become turbulent because of the vapor bubbles (Figure 6B). Because the vapor bubbles cannot stay on the hydrophilic surfaces, many vapor bubbles vent from the surfaces, and the droplet ejection increases (Figure 6C). If the surface temperature continues to rise, the vapor bubbles generated on the side of the micropillars can coalesce to a vapor mattress and avoid part of the contact between the droplet and the surface. The droplet thus moves up (Figure 6D). The water CA on the surfaces with micropillars can be estimated by eq 3

$$\cos\theta_r^w = r\cos\theta = \left[1 + \frac{4a_1H_1}{(a_1 + b_1)^2}\right]\cos\theta \tag{3}$$

Where r is the roughness of the microstructures. a_1, b_1, and H_1 are the width, spacing and height of the micropillars, respectively (see the schematic diagram in Supporting Information, S8). θ_r^w and θ are the apparent contact angle at Wenzel state and the intrinsic contact angle.

With the constant spacing and height of the micropillars, the roughness (r) of micropillars with width of 5, 10, and 15 μm are 1.44, 1.50 and 1.48, respectively. When MSis surface with ~10 μm pillars achieved the highest MCAs, MEAs and T_{trans} (Figure 3d), these surfaces are the roughest, and their θ_r^w is the lowest. However, the MCAs, MEAs, and T_{trans} on ~15 μm wide micropillars were the lowest (Figure 3c), whereas their θ_r^w is not the highest. Therefore, only the wettability of the surfaces could not give a complete understanding on the influence of chemical compounds and micro/nano rough structures on the in site wetting transition process.

As known, after the droplet processes a partial wetting state (Wenzel–Cassie intermediate), only when the vapor mattress is thick enough does the droplet block the vapor mattress and bounce from the surface and the droplet does not wet the surfaces at all (Cassie state) (Figure 6E). In fact, the contact states of the droplets on the heated surfaces play an important role on the wetting transition processes.[45] The scheme of the possible contact state is illustrated in Figure 6F. The liquid–vapor interface is concave outward on the unmodified rough surface, and the surface tension acts in the same direction as gravity for a hydrophilic surface. The local wetting force acting around each pillar can be calculated by $f_w = \pi a_1\gamma_{LV}$. Therefore, the global average wetting force, F_W, acting on the droplet as a resistance force of droplet recoil can be calculated using eq 4

$$F_w = \left(\frac{\pi R_{base}^2}{(a_1 + b_1)^2}\right)\pi a_1\gamma_{LV}\cos\theta \tag{4}$$

Where $((\pi R_{base}^2)/(a_1 + b_1)^2)$ accounts for the number of pillars in contact with the droplet base area (i.e., πR_{base}^2 = MCA), and γ_{LV} is the interfacial liquid–vapor surface tension of water at 100 °C. The high-pressure vapor mattress beneath the droplet provides the nonwetting force. Only if the vapor mattress beneath the droplet is high enough, (i.e., $P_{vap} > P_{lip} > P_{amb}$), the droplets rebound. Therefore, on the superhydrophilic surfaces, the combination of the larger contact area (MCA) of the droplets and the lowest $(a_1/(a_1 + b_1)^2)$ of micropillars (which agree well with the Wenzel state formulation eq 3), is always accompanied by the highest T_{trans}. Besides, the MCA will increases with the decrease of static contact angle below the wetting limit temperatures.[46]

If decrease a_1 and b_1 decrease to nanoscale, F_w will increase sharply. Thus, the MCAs, MEAs and T_{trans} rose significantly. If the nanowire arrays were constructed on the MSis surface (i.e., MNSis surface), it was found that the larger the nanowire array areas, the more the MCAs and MEAs were improved. However, T_{trans} could not increase markedly because the F_w was dominated by microscaled structure.

On the FAS-modified rough surface at room temperature, the rough structures cannot be completely wetted by the liquid. In turn, there is an air mattress trapped between the surface and the liquid—the droplet is at a Cassie state (Figure 6a). If the surface is heated, the vapor bubbles can generate at limit contact area, and then they pin the contact area. The tiny vapor bubbles cannot coalesce with the air mattress, and the liquid droplets stand on the surface at a Wenzel–Cassie intermediate state (Figure 6b). With increasing surface temperature, the pinned vapor bubbles grow in site, and they will coalesce with the trapped air layer to form a mixture mattress when the three contact phase lines (TPCL) moves up (Figure 6c, d). When the TPCL move to the top of the rough structures, the pinned vapor bubbles on the top coalesce with the gas mixture mattress to form a continuous gas layer. The mixture gas mattress prevents contact between the liquid and the surface, and the droplet rebounds from the surface (Figure 6e). For a typical superhydrophobic surface, the curvature of the liquid–vapor interface is concave inward counteracting wetting, as schematically shown in Figure 6f. The surface tension acts in the opposite direction as gravity for a hydrophobic surface. The F_W acting on the droplet will be a nonwetting force for the droplet rebound. The T_{trans} on structured surfaces is much lower than that on the FAS-SSis.

On the superhydrophobic surfaces with micropillars, the T_{trans} reach the lowest value when the $(a_1/(a_1 + b_1)^2)$ is the smallest.

Although nanowires could provide more nucleation cites for vapor bubbles and possess larger F_w, the vapor bubbles adhered on the tips of the nanowires, and could not form continuous vapor layers if the surface temperature was not high enough.

The spaces between the microstructures were more useful at entrapping air to form a thick air layer. The water CA on the FAS-modified surfaces with micropillars can be estimated by eq 5.

$$\cos\theta_r^c = A_1(1 + \cos\theta) - 1 \tag{5}$$

where

$$A_1 = \frac{1}{(b_1/a_1 + 1)^2}$$

a_1 and b_1 are the width and spacing of the micropillars, respectively. θ_r^c and θ are the apparent contact angle at Cassie state and the intrinsic contact angle.

It can be found that the θ_r^c will reach the largest value when the a_1 is the lowest. Thus, the microstructures best reduced the T_{trans} when the micropillars are ~5 μm wide.

If the micro/nano hierarchical structures were constructed, the θ_r^c will reach 180° and the gas layer could be form at very low temperatures. Thus, on the FAS-MNSis surfaces, we found

that the MCAs are reduced with increasing surface temperature and the MEAs were always zero.

4. CONCLUSION

We studied the wetting behavior of liquid droplets on four kinds of micro- and nanostructured surfaces with different chemical components. Parameters of interest include the MCAs, the MEAs and the T_{trans}. Experimental results demonstrate that both the MCAs and MEAs decreased with increasing surface temperature. When the MEAs drop to zero at a critical temperature (T_{trans}), the droplets rebound from the heated surfaces. The chemical compounds and rough surface structures are crucial to the droplets' wetting transition behaviors. When the droplets impact the unmodified surfaces, microstructures increase the MCAs, MEAs and T_{trans}. The MCAs are especially increased more at high temperatures close to T_{trans}. However, the microstructures are less effective at increasing MEAs and T_{trans} than nanostructures. After FAS-modification, both the nano and microstructures reduce the T_{trans}. On the FAS-MNSis surfaces, the MEAs were always zero, i.e., the droplets rebounded at room temperature and the wetting transition did not take place.

The two proposed mechanisms of wetting at high temperature explain the transition phenomena well. The liquid−vapor interface is concave outward on the unmodified rough surface making the surface tension act resistant force during dewetting process while it is concave inward on the FAS-modified rough surface making the surface tension act driving force. The high-pressure vapor cushion beneath the droplet are essential for the wetting transition behaviors on the surfaces before FAS-modification, while the trapped air mattress is the most important factor after FAS-modification. This high-temperature wetting transition could be potentially valuable in industrial applications including improving heat transfer efficiency during spray cooling, the material choice in liquid−solid systems working at nonambient temperatures, and high duty lubrication.

■ ASSOCIATED CONTENT

Supporting Information

Schematic of the experimental device, SEM top view and side view images of micro and micro/nanocomposite structures, and calculation of the roughness r of the silicon surfaces with different micropillars. This material is available free of charge via the Internet at http://pubs.acs.org.

■ AUTHOR INFORMATION

Corresponding Author

*E-mail: wangjm@buaa.edu.cn.

Author Contributions

The manuscript was written through contributions of all authors. All authors have given approval to the final version of the manuscript.

Notes

The authors declare no competing financial interest.

■ ACKNOWLEDGMENTS

We are grateful to the financial support from National Natural Science Foundation of China (20901006, 21121001, 91127025), National Basic Research Program of China (2012CB933202), the Key Research Program of the Chinese Academy of Sciences (KJZD-EW-M01), and the 111 project (B14009).

■ REFERENCES

(1) Mudawar, I. Assessment of High-Heat-Flux Thermal Management Schemes. *IEEE Trans. Compon. Packag. Technol.* **2001**, *24*, 122−141.
(2) Kang, M. G. Experimental Investigationof Tube Length Effect on Nucleate Pool Boiling Heat Transfer. *Ann. Nucl. Energy.* **1998**, *25*, 295−304.
(3) Chaudhari, M.; Puranik, B.; Agrawal, A. Heat Transfer Characteristics of Synthetic Jet Impingement Cooling. *Int. J. Heat Mass Transfer* **2010**, *53*, 1057−1069.
(4) Chiu, H. C.; Jang, J. H.; Yeh, H. W.; Wu, M. S. The Heat Transfer Characteristics of Liquid Cooling Heatsink Containing Microchannels. *Int. J. Heat Mass Transfer* **2011**, *54*, 34−42.
(5) Silieti, M.; Divo, E.; Kassab, A. J. The Effect of Conjugate Heat Transfer on Film Cooling Effectiveness. *Numer. Heat Transfer, Part B* **2010**, *56*, 335−350.
(6) Martínez, G. E.; Antóna, R.; Ramosa, J. C.; Khodabandeh, R. Influence of Surface Roughness on a Spray Cooling System with R134a. Part I: Heat Transfer Measurements. *Exp. Therm Fluid Sci.* **2013**, *46*, 183−190.
(7) Zhang, Z.; Li, J.; Jiang, P. X. Experimental Investigation of Spray Cooling on Flat and Enhanced Surfaces. *Appl. Therm. Eng.* **2013**, *51*, 102−111.
(8) Xie, J. L.; Tan, Y. B.; Duan, F.; Ranjith, K.; Wong, T. N.; Toh, K. C.; Chan, P. K. Study of Heat Transfer Enhancement for Structured Surfaces in Spray Cooling. *Appl. Therm. Eng.* **2013**, *59*, 464−472.
(9) Kim, J. H.; You, S. M.; Choi, S. U. Evaporative Spray Cooling of Plain and Microporous Coated Surfaces. *Int. J. Heat Mass Transfer* **2004**, *47*, 3307−3315.
(10) Li, D.; Wu, G. S.; Wang, W.; Wang, Y. D.; Liu, D.; Zhang, D. C.; Chen, Y. F.; Peterson, G. P.; Yang, R. Enhancing Flow Boiling Heat Transfer in Microchannels for Thermal Management with Monolithically-Integrated Silicon Nanowires. *Nano Lett.* **2012**, *12*, 3385−3390.
(11) Yang, F.; Dai, X.; Kuo, C. J.; Peles, Y.; Khan, J.; Li, C. Enhanced Flow Boiling in Microchannels by Self-Sustained High Frequency Two-Phase Oscillations. *Int. J. Heat Mass Transfer* **2013**, *58*, 402−412.
(12) Chen, R.; Lu, M.; Srinivasan, V.; Wang, Z.; Cho, H. H.; Majumdar, A. Nanowires for Enhanced Boiling Heat Transfer. *Nano Lett.* **2009**, *9*, 548−553.
(13) Li, C.; Wang, Z.; Wang, P. I.; Peles, Y.; Koratkar, N.; Peterson, G. P. Nanostructured Copper Interfaces for Enhanced Boiling. *Small* **2008**, *4*, 1084−1088.
(14) Yao, X.; Chen, Q.; Xu, L.; Li, Q.; Song, Y.; Gao, X.; Quéré, D.; Jiang, L. Bioinspired Ribbed Nanoneedles with Robust Superhydrophobicity. *Adv. Funct. Mater.* **2010**, *20*, 656−662.
(15) Yao, X.; Song, Y.; Jiang, L. Applications of Bio-Inspired Special Wettable Surfaces. *Adv. Mater.* **2011**, *23*, 719−734.
(16) Tian, Y.; Jiang, L. Wetting: Intrinsically Robust Hydrophobicity. *Nat. Mater.* **2013**, *12*, 291−292.
(17) Bai, H.; Ju, J.; Zheng, Y.; Jiang, L. Functional Fibers with Unique Wettability Inspired by Spider Silks. *Adv. Mater.* **2012**, *24*, 2786−2791.
(18) O'Hanley, H.; Coyle, C.; Buongiorno, J.; McKrell, T.; Hu, L.; Rubner, M.; Cohen, R. Separate Effects of Surface Roughness, Wettability, and Porosity on the Boiling Critical Heat Flux. *Appl. Phys. Lett.* **2013**, *103*, 024102.
(19) Yang, J.; Zhang, Z.; Men, X.; Xu, X.; Zhu, X. Thermo-Responsive Surface Wettability on a Pristine Carbon Nanotube Film. *Carbon* **2011**, *49*, 19−23.
(20) Betz, A. R.; Jenkins, J.; Kim, C. J.; Attinger, D. Boiling Heat Transfer on Superhydrophilic, Superhydrophobic, and Superbiphilic Surfaces. *Int. J. Heat Mass Transfer* **2013**, *57*, 733−741.
(21) Kim, S. J.; Bang, I. C.; Buongiorno, J.; Hu, L. W. Effects of Nanoparticle Deposition on Surface Wettability Influencing Boiling Heat Transfer in Nanofluids. *Appl. Phys. Lett.* **2006**, *89*, 153107.

(22) Duursma, G.; Sefiane, K.; Kennedy, A. Experimental Studies of Nanofluid Droplets in Spray Cooling. *Heat Transfer Eng.* **2009**, *30*, 1108−1120.
(23) Quéré, D. Leidenfrost Dynamics. *Annu. Rev. Fluid Mech.* **2013**, *45*, 197−215.
(24) Vakarelski, I. U.; Marston, J. O.; Chan, D. Y.; Thoroddsen, S. T. Drag Reduction by Leidenfrost Vapor Layers. *Phys. Rev. Lett.* **2011**, *106*, 214501.
(25) Dupeux, G.; Merrer, M. L.; Clanet, C.; Quéré, D. Trapping Leidenfrost Drops with Crenelations. *Phys. Rev. Lett.* **2011**, *107*, 114503.
(26) Liu, G.; Craig, V. S. Macroscopically Flat and Smooth Superhydrophobic Surfaces: Heating Induced Wetting Transitions up to the Leidenfrost Temperature. *Faraday Discuss.* **2010**, *146*, 141−151.
(27) Tsai, P.; Lammertink, R. G.; Wessling, M.; Lohse, D. Evaporation-Triggered Wetting Transition for Water Droplets upon Hydrophobic Microstructures. *Phys. Rev. Lett.* **2010**, *104*, 116102.
(28) Kim, H.; Truong, B.; Buongiorno, J.; Hu, L. W. On the Effect of Surface Roughness Height, Wettability, and Nanoporosity on Leidenfrost Phenomena. *Appl. Phys. Lett.* **2011**, *98*, 083121.
(29) Kim, H.; Truong, B.; Buongiorno, J.; Hu, L. W. Effects of Micro/Nano-Scale Surface Characteristics on the Leidenfrost Point Temperature of Water. *J. Therm. Sci. Technol.* **2012**, *7*, 453−462.
(30) Zhang, T.; Wang, J.; Chen, L.; Zhai, J.; Song, Y.; Jiang, L. High-Temperature Wetting Transition on Micro-and Nanostructured Surfaces. *Angew. Chem., Int. Ed.* **2011**, *50*, 5311−5314.
(31) Vakarelski, I. U.; Patankar, N. A.; Marston, J. O.; Chan, D. Y.; Thoroddsen, S. T. Stabilization of Leidenfrost Vapour Layer by Textured Superhydrophobic Surfaces. *Nature* **2012**, *489*, 274−277.
(32) Bird, J. C.; Dhiman, R.; Kwon, H. M.; Varanasi, K. K. Reducing the Contact Time of a Bouncing Drop. *Nature* **2013**, *503*, 385−388.
(33) Sen, S.; Vaikuntanathan, V.; Sivakumar, D. Experimental Investigation of Biofuel Drop Impact on Stainless Steel Surface. *Exp. Therm Fluid Sci.* **2014**, *54*, 38−46.
(34) Maksimov, A. O.; Kaverin, A. M.; Baidakov, V. G. Heterogeneous Vapor Bubble Nucleation on a Rough Surface. *Langmuir* **2013**, *29*, 3924−3934.
(35) Kapsenberg, F.; Strid, L.; Thiagarajan, N.; Narayanan, V.; Bhavnani, S. H. On the Lateral Fluid Motion During Pool Boiling Via Preferentially Located Cavities. *Appl. Phys. Lett.* **2014**, *104*, 154105.
(36) Wang, J.; Zheng, Y.; Nie, F.; Zhai, J.; Jiang, L. Air Bubble Bursting Effect of Lotus Leaf. *Langmuir* **2009**, *25*, 14129−14134.
(37) Wang, J.; Yang, Q.; Wang, M.; Wang, C.; Jiang, L. Rose Petals with a Novel and Steady Air Bubble Pinning Effect in Aqueous Media. *Soft Mater.* **2012**, *8*, 2261−2266.
(38) Kandlikar, S. G. Controlling Bubble Motion over Heated Surface Through Evaporation Momentum Force to Enhance Pool Boiling Heat Transfer. *Appl. Phys. Lett.* **2013**, *102*, 051611.
(39) Nair, H.; Staat, H. J.; Tran, T.; van Houselt, A.; Prosperetti, A.; Lohse, D.; Sun, C. The Leidenfrost Temperature Increase for Impacting Droplets on Carbon-nanofiber Surfaces. *Soft Matter* **2014**, *10*, 2102−2109.
(40) Kim, S. H.; Ahn, S. H.; Kim, J.; Kaviany, M.; Kim, H. M. Dynamics of Water Droplet on a Heated Nanotubes Surface. *Appl. Phys. Lett.* **2013**, *102*, 233901.
(41) Lv, J.; Song, Y.; Jiang, L.; Wang, J. Bio-Inspired Strategies for Anti-Icing. *ACS Nano* **2014**, *8*, 3152−3169.
(42) Negeed, E.-S. R.; Albeirutty, M.; Takata, Y. Dynamic Behavior of Micrometric Single Water Droplets Impacting onto Heated Surfaces with TiO_2 Hydrophilic Coating. *Int. J. Therm Sci.* **2014**, *79*, 1−17.
(43) Tran, T.; Staat, H. J. J.; Prosperetti, A. Drop Impact on Superheated Surfaces. *Phys. Rev. Lett.* **2012**, *108*, 036101.
(44) Tsai, P.; Pacheco, S.; Pirat, C. Drop Impact upon Micro- and Nanostructured Superhydrophobic Surfaces. *Langmuir* **2009**, *25*, 12293−12298.
(45) Adera, S.; Raj, R.; Enright, R.; Wang, E. N. Non-wetting Droplets on Hot Superhydrophilic Surfaces. *Nat. Commun.* **2013**, *4*, 2518−2524.
(46) Deendarlianto; Takata, Y.; Hidaka, S.; Indarto; Widyaparaga, A.; Kamal, S.; Purnomo; Kohno, M. Effect of Static Contact Angle on the Droplet Dynamics during the Evaporation of a Water Droplet on the Hot Walls. *Int. J. Heat Mass Transfer* **2014**, *71*, 691−705.